

## Supporting information

---

### **High-density formation of Ir/MoO<sub>x</sub> interface through hybrid clustering for chemoselective nitrostyrene hydrogenation**

Shun Hayashi<sup>\*a</sup> and Tetsuya Shishido<sup>bcd</sup>

<sup>a</sup>Division of Physical Sciences, Department of Science and Engineering, National Museum of Nature and Science, Ibaraki 305-0005, Japan

<sup>b</sup>Department of Applied Chemistry for Environment, Graduate School of Urban Environmental Sciences, Tokyo Metropolitan University, Tokyo 192-0397, Japan

<sup>c</sup>Research Center for Hydrogen Energy-Based Society, Tokyo Metropolitan University, Tokyo 192-0397, Japan

<sup>d</sup>Elements Strategy Initiative for Catalysts & Batteries, Kyoto University, Kyoto 615-8520, Japan

E-mail: s-hayashi@kahaku.go.jp (SH)

---

## List of Figures

- S1. (a) Positive-ion ESI-MS and (b) FT-IR spectra of [(IrCp\*)<sub>4</sub>Mo<sub>4</sub>O<sub>16</sub>].
- S2. (a) Positive-ion ESI-MS and (b) FT-IR spectra of [(IrCp\*)<sub>4</sub>V<sub>6</sub>O<sub>19</sub>].
- S3. Ir L<sub>3</sub>-edge EXAFS of (i) Ir<sub>4</sub>Mo<sub>4</sub>/Al<sub>2</sub>O<sub>3</sub>, (ii) Ir-Mo/Al<sub>2</sub>O<sub>3</sub>, and (iii) [(IrCp\*)<sub>4</sub>Mo<sub>4</sub>O<sub>16</sub>].
- S4. Ir L<sub>3</sub>-edge in situ XANES spectra of (a) Ir<sub>4</sub>Mo<sub>4</sub>/Al<sub>2</sub>O<sub>3</sub>\_ads under O<sub>2</sub>/He flow and (b) Ir<sub>4</sub>Mo<sub>4</sub>/Al<sub>2</sub>O<sub>3</sub>\_air(573) under H<sub>2</sub> flow. Mo K-edge in situ XANES spectra of (c) Ir<sub>4</sub>Mo<sub>4</sub>/Al<sub>2</sub>O<sub>3</sub>\_ads under O<sub>2</sub>/He flow and (d) Ir<sub>4</sub>Mo<sub>4</sub>/Al<sub>2</sub>O<sub>3</sub>\_air(573) under H<sub>2</sub> flow.
- S5. TG-DTA of [(IrCp\*)<sub>4</sub>Mo<sub>4</sub>O<sub>16</sub>].
- S6. (a) Ir L<sub>3</sub>- and (b) Mo K-edge in situ XANES spectra of Ir<sub>4</sub>Mo<sub>4</sub>/Al<sub>2</sub>O<sub>3</sub> under H<sub>2</sub> flow. (c) Ir L<sub>3</sub>- and (d) Mo K-edge in situ XANES spectra of Ir-Mo/Al<sub>2</sub>O<sub>3</sub> under H<sub>2</sub> flow.
- S7. Double logarithmic plot of the initial reaction rate of NB hydrogenation over Ir<sub>4</sub>Mo<sub>4</sub>/Al<sub>2</sub>O<sub>3</sub> as a function of (a) [NB] and (b) P<sub>H2</sub>. Double logarithmic plot of the initial reaction rate of ST hydrogenation over Ir<sub>4</sub>Mo<sub>4</sub>/Al<sub>2</sub>O<sub>3</sub> as a function of (c) [ST] and (d) P<sub>H2</sub>.
- S8. Double logarithmic plot of the initial reaction rate of NB hydrogenation over Ir-Mo/Al<sub>2</sub>O<sub>3</sub> as a function of (a) [NB] and (b) P<sub>H2</sub>. Double logarithmic plot of the initial reaction rate of ST hydrogenation over Ir-Mo/Al<sub>2</sub>O<sub>3</sub> as a function of (c) [ST] and (d) P<sub>H2</sub>.
- S9. Representative GC chart of hydrogenation of **1** catalyzed by (a) Ir<sub>4</sub>Mo<sub>4</sub>/TiO<sub>2</sub> and (b) Ir-Mo/TiO<sub>2</sub>.

## List of Tables

- S1. Structural parameters obtained from the curve-fitting analysis of the Ir L<sub>3</sub>-edge FT-EXAFS data.
- S2. Dependence of hydrogenation activity on the reduction temperature of Ir-Mo-based catalysts.
- S3. Hydrogenation of **1** catalyzed by Ir-based catalysts.
- S4. Reaction orders of hydrogenation of NB and ST.

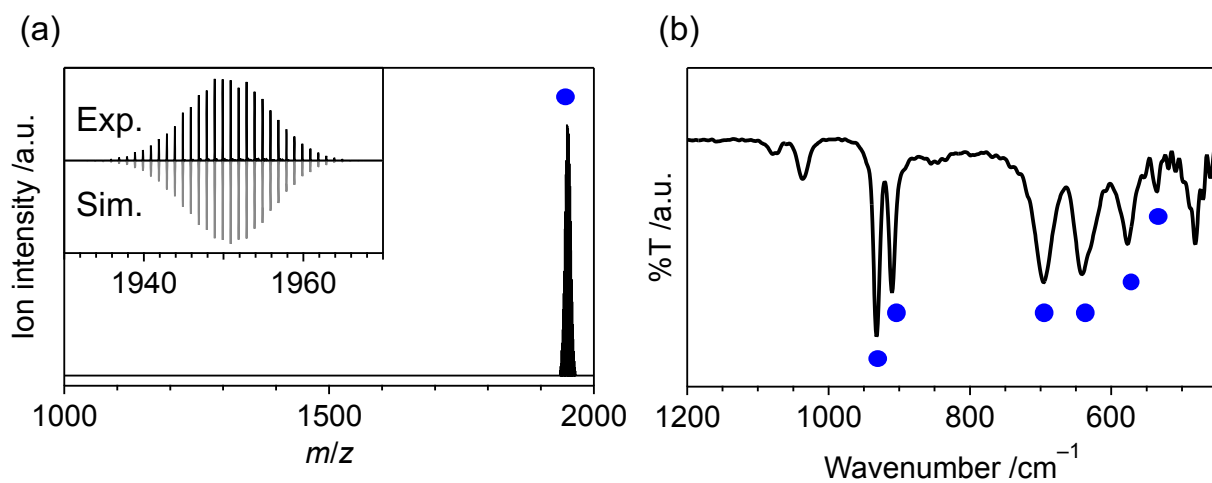


Figure S1. (a) Positive-ion ESI-MS and (b) FT-IR spectra of  $[(\text{IrCp}^*)_4\text{Mo}_4\text{O}_{16}]$ .

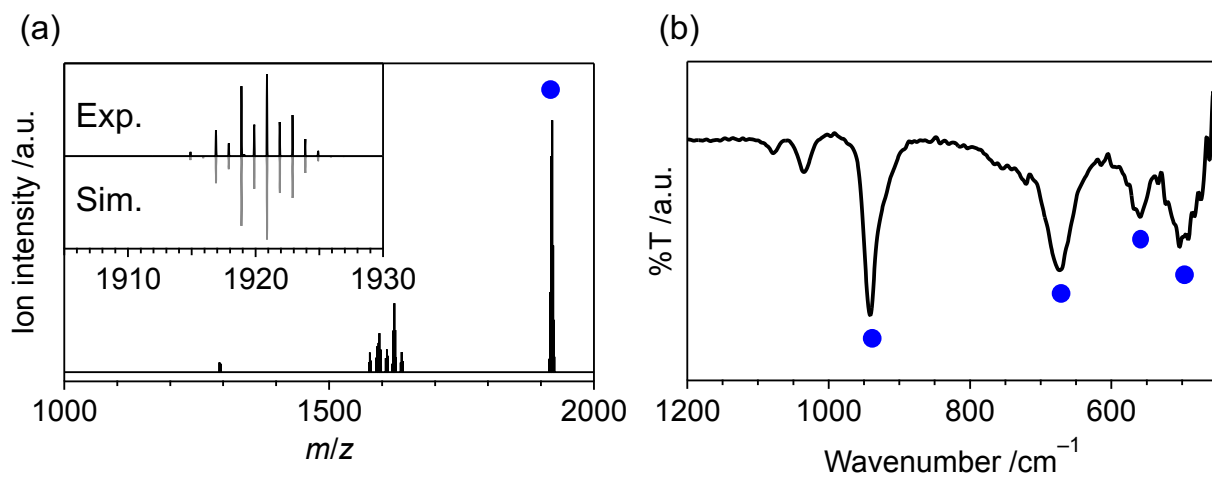


Figure S2. (a) Positive-ion ESI-MS and (b) FT-IR spectra of  $[(\text{IrCp}^*)_4\text{V}_6\text{O}_{19}]$ .

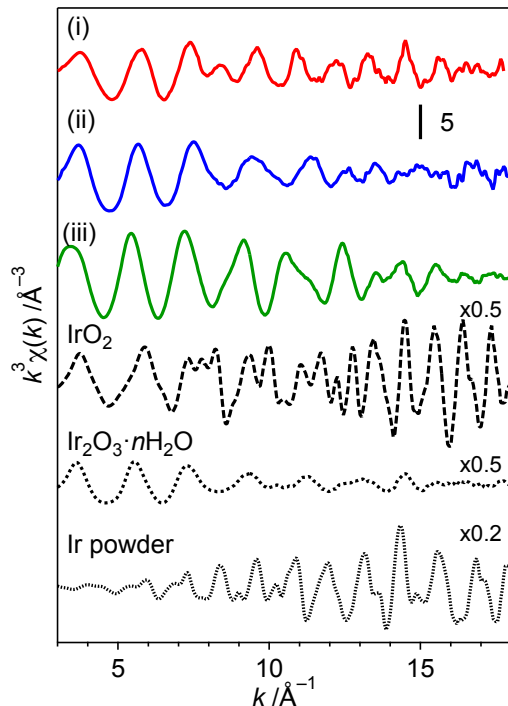


Figure S3. Ir L<sub>3</sub>-edge EXAFS spectra of (i) Ir<sub>4</sub>Mo<sub>4</sub>/Al<sub>2</sub>O<sub>3</sub>, (ii) Ir-Mo/Al<sub>2</sub>O<sub>3</sub>, and (iii) [(IrCp\*)<sub>4</sub>Mo<sub>4</sub>O<sub>16</sub>].

Table S1. Structural parameters obtained from the curve-fitting analysis of the Ir L<sub>3</sub>-edge FT-EXAFS data.

Compound	Bonds	CN*	$r / \text{\AA}^\dagger$	$\sigma^2 / 10^{-3} \text{\AA}^{2\ddagger}$	$R / \%^\S$
Ir powder <sup>a</sup>	Ir-Ir	12(2)	2.710(6)	3.7(5)	13.0
Ir <sub>2</sub> O <sub>3</sub> · <i>n</i> H <sub>2</sub> O <sup>b</sup>	Ir-O	5.6(6)	2.044(8)	6.2(9)	1.7
IrO <sub>2</sub> <sup>c</sup>	Ir-O	6(1)	1.987(6)	3(1)	10.7
	Ir-Ir	4(3)	3.154(9)	4(3)	
	Ir-Ir	4(2)	3.550(5)	2(1)	
[(IrCp*) <sub>4</sub> Mo <sub>4</sub> O <sub>16</sub> ] <sup>c</sup>	Ir-O	6.2(6)	2.112(7)	3.8(7)	13.3
	Ir-Mo	0.8(4)	3.272(8)	2(1)	
Ir <sub>4</sub> Mo <sub>4</sub> /Al <sub>2</sub> O <sub>3</sub>	Ir-O	3.2(5)	2.040(6)	7(1)	13.1
<u>Air(573)H<sub>2</sub>(573)</u> <sup>a</sup>	Ir-Ir	3.8(8)	2.688(4)	7.6(8)	
Ir-Mo/Al <sub>2</sub> O <sub>3</sub>	Ir-O	4.9(5)	2.002(9)	6.4(9)	7.0
<u>Air(573)H<sub>2</sub>(573)</u> <sup>b</sup>					

\*Coordination number. †Bond length. ‡Debye-Waller factor.

$\S R = (\sum(k^3\chi^{\text{data}}(k) - k^3\chi^{\text{fit}}(k))^2)^{1/2} / (\sum(k^3\chi^{\text{data}}(k))^2)^{1/2}$ .

$r$  range of the curve-fitting analysis: <sup>a</sup>1.4–2.9 Å; <sup>b</sup>1.4–2.0 Å; <sup>c</sup>1.4–3.8 Å.

Table S2. Dependence of hydrogenation activity on the reduction temperature of Ir-Mo-based catalysts.<sup>a</sup>

Entry	Catalyst	Red. Temp. /K	Time /min	Conv. /%	Select. /%		
					2	3	4
1-1	Ir <sub>4</sub> Mo <sub>4</sub> /TiO <sub>2</sub>	573	10	63	96	1	3
1-2		773		61	98	1	1
2-1	Ir <sub>4</sub> Mo <sub>4</sub> /Al <sub>2</sub> O <sub>3</sub>	573	20	48	96	2	2
2-2		773		39	97	2	1
3-1	Ir-Mo/TiO <sub>2</sub>	573	10	72	72	6	22
3-2		773		66	87	3	9
4-1	Ir-Mo/Al <sub>2</sub> O <sub>3</sub>	573	20	35	63	12	25
4-2		773		44	67	8	25

<sup>a</sup>Reaction conditions: **1** (0.1 mmol), H<sub>2</sub> (0.3 MPa), toluene (1 mL), catalyst (10 mg, Ir:0.52 mol%), and 303 K.

Table S3. Hydrogenation of **1** catalyzed by Ir-based catalysts<sup>a</sup>

Entry	Catalyst	Ir loading /wt%	Time /min	Conv. /%	Select. /%			
					2	3	4	
1-1	Ir <sub>4</sub> Mo <sub>4</sub> /Al <sub>2</sub> O <sub>3</sub>	1	10	26	97	2	1	
1-2			60	91	94	2	4	
1-3			10	18	97	2	1	
1-4			90	90	95	2	3	
2	Ir <sub>4</sub> V <sub>6</sub> /Al <sub>2</sub> O <sub>3</sub>	1	10	20	87	11	2	
3	Ir-Mo/Al <sub>2</sub> O <sub>3</sub>	1	10	24	63	12	25	
4	Ir-V/Al <sub>2</sub> O <sub>3</sub>	1	10	40	55	12	33	
5	Ir/Al <sub>2</sub> O <sub>3</sub>	1	10	42	42	17	41	
6-1	Ir/MoO <sub>3</sub>	0.1	30	32	98	1	<1	
6-2			0.3	30	39	95	1	4
6-3			1	30	19	73	22	4
6-4			5	30	16	26	69	5
7-1	Ir <sub>4</sub> Mo <sub>4</sub> /TiO <sub>2</sub> <sup>b</sup>	1	5	29	99	<1	<1	
7-2			20	97	94	<1	6	
8	Ir-Mo/TiO <sub>2</sub> <sup>b</sup>	1	5	40	93	3	4	

<sup>a</sup>Reaction conditions: **1** (0.1 mmol), H<sub>2</sub> (0.3 MPa), toluene (1 mL), catalyst (2–100 mg, Ir:0.52 mol%), and 303 K. <sup>b</sup>Reduction temperature: 773 K.

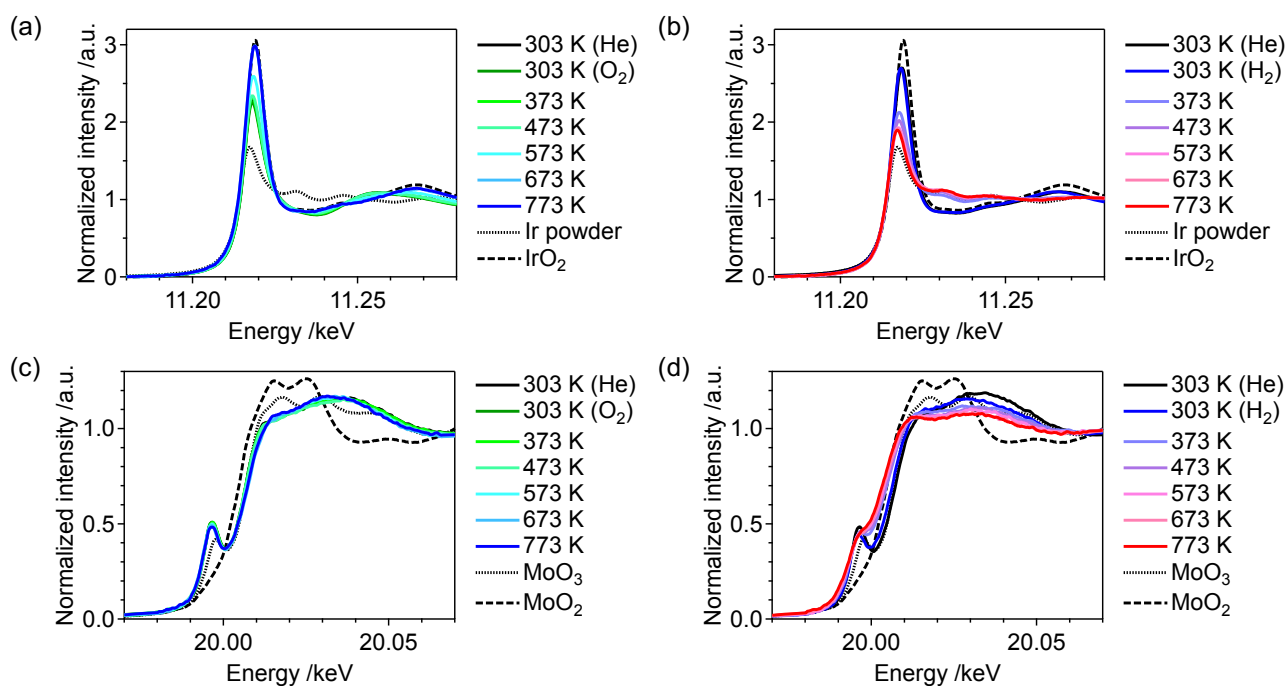


Figure S4. Ir L<sub>3</sub>-edge in situ XANES spectra of (a) Ir<sub>4</sub>Mo<sub>4</sub>/Al<sub>2</sub>O<sub>3</sub>\_ads under O<sub>2</sub>/He flow and (b) Ir<sub>4</sub>Mo<sub>4</sub>/Al<sub>2</sub>O<sub>3</sub>\_air(573) under H<sub>2</sub> flow. Mo K-edge in situ XANES spectra of (c) Ir<sub>4</sub>Mo<sub>4</sub>/Al<sub>2</sub>O<sub>3</sub>\_ads under O<sub>2</sub>/He flow and (d) Ir<sub>4</sub>Mo<sub>4</sub>/Al<sub>2</sub>O<sub>3</sub>\_air(573) under H<sub>2</sub> flow.

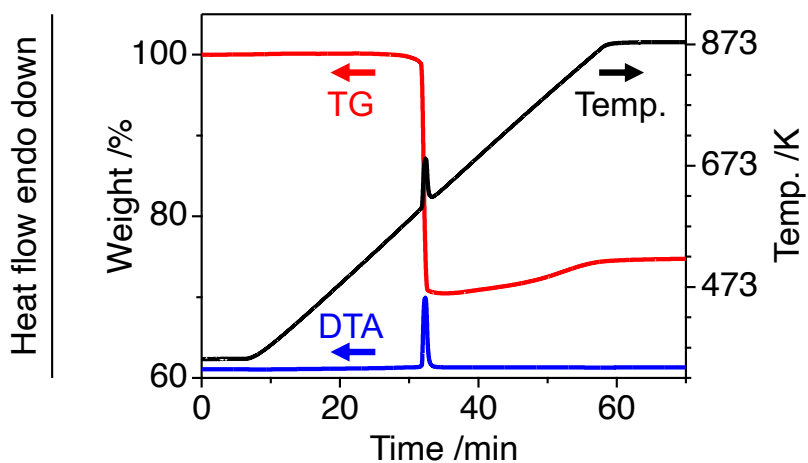


Figure S5. TG-DTA of [(IrCp\*)<sub>4</sub>Mo<sub>4</sub>O<sub>16</sub>].

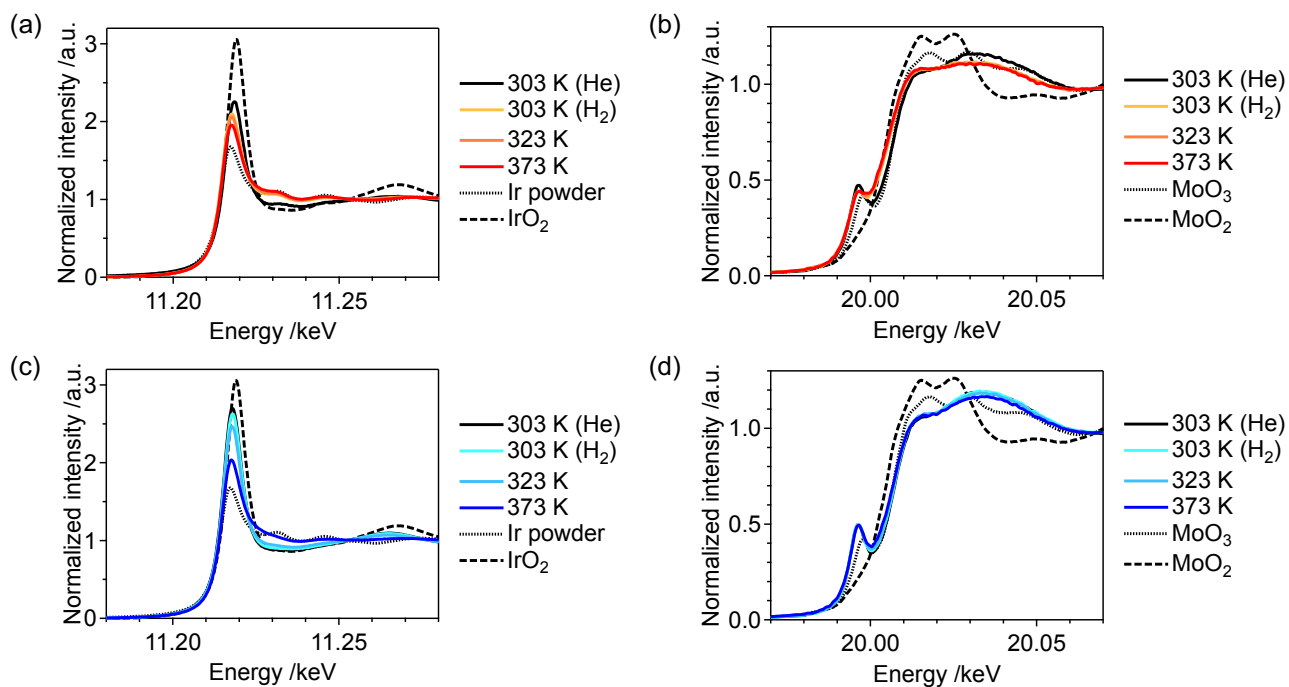


Figure S6. (a) Ir L<sub>3</sub>- and (b) Mo K-edge in situ XANES spectra of Ir<sub>4</sub>Mo<sub>4</sub>/Al<sub>2</sub>O<sub>3</sub> under H<sub>2</sub> flow. (c) Ir L<sub>3</sub>- and (d) Mo K-edge in situ XANES spectra of Ir-Mo/Al<sub>2</sub>O<sub>3</sub> under H<sub>2</sub> flow.

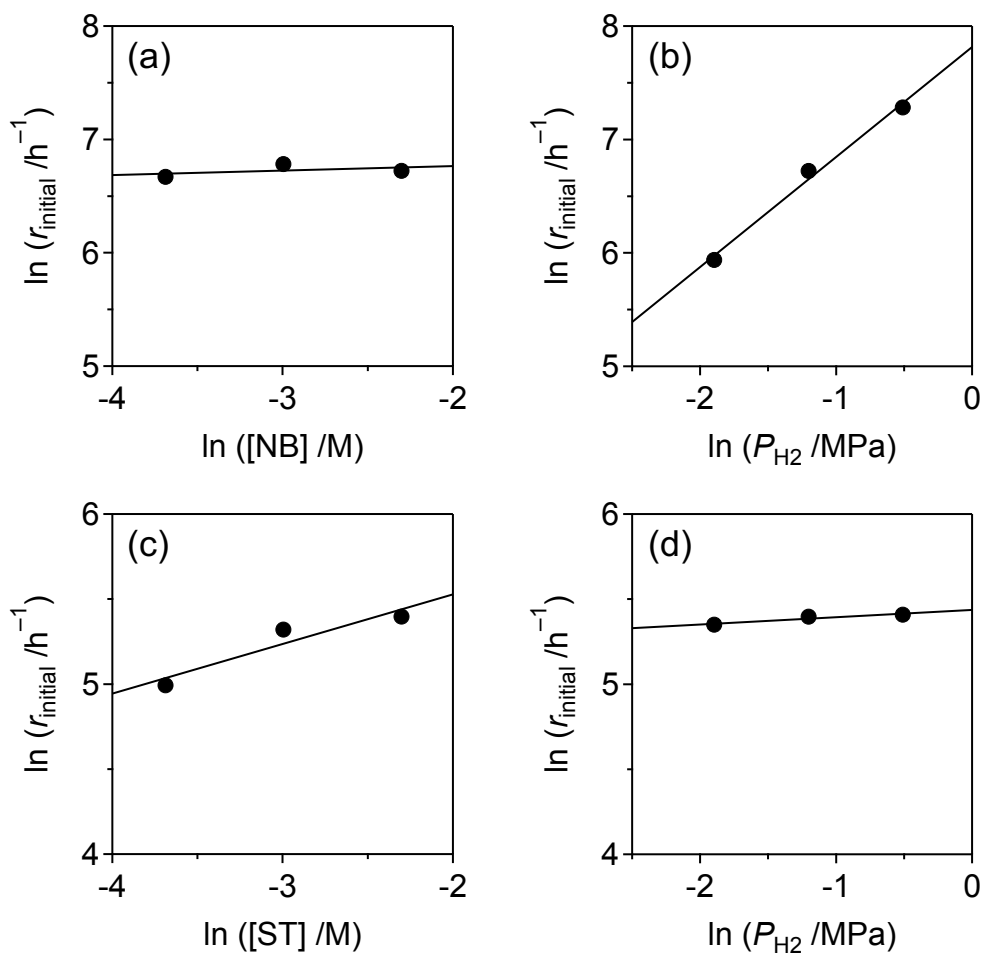


Figure S7. Double logarithmic plot of the initial reaction rate of NB hydrogenation over Ir<sub>4</sub>Mo<sub>4</sub>/Al<sub>2</sub>O<sub>3</sub> as a function of (a) [NB] and (b)  $P_{\text{H}_2}$ . Double logarithmic plot of the initial reaction rate of ST hydrogenation over Ir<sub>4</sub>Mo<sub>4</sub>/Al<sub>2</sub>O<sub>3</sub> as a function of (c) [ST] and (d)  $P_{\text{H}_2}$ . Reaction conditions: NB or ST (0.025–0.1 mmol), H<sub>2</sub> (0.15–0.6 MPa), toluene (1 mL), Ir<sub>4</sub>Mo<sub>4</sub>/Al<sub>2</sub>O<sub>3</sub> (10 mg, Ir: 0.52 mol%), and 303 K.



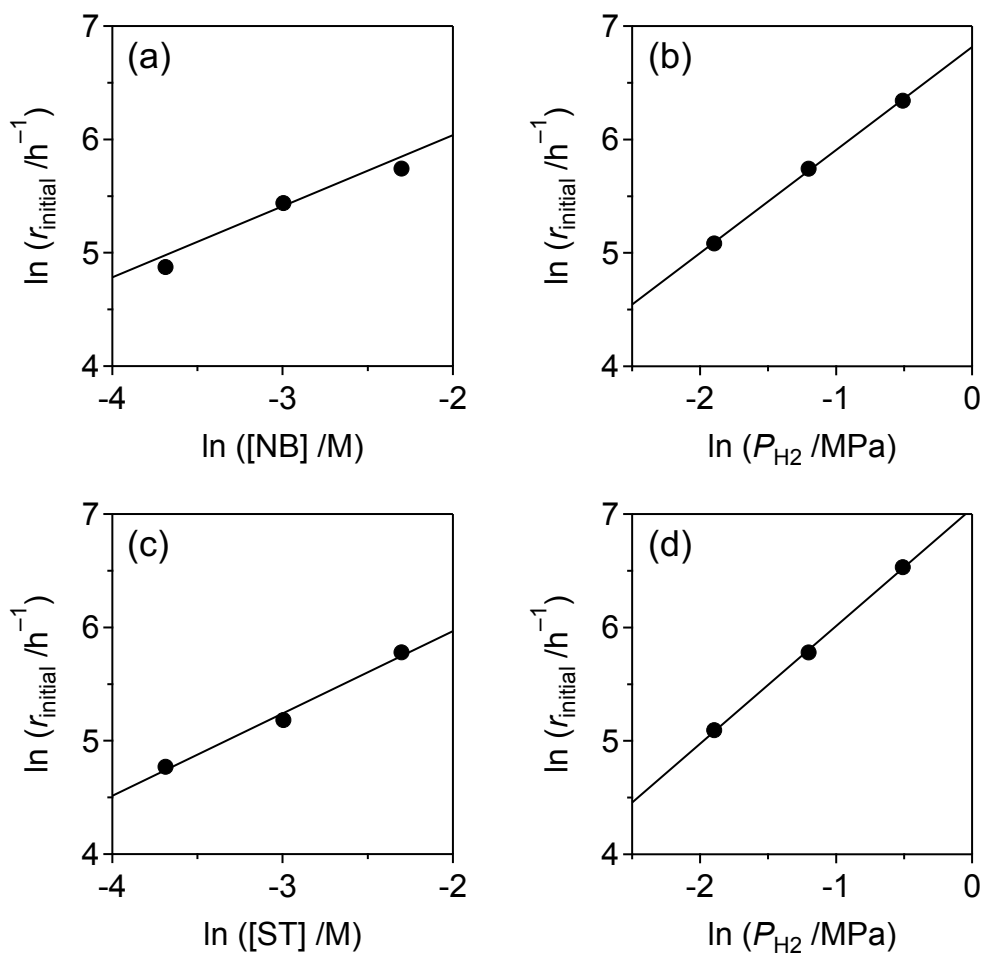


Figure S8. Double logarithmic plot of the initial reaction rate of NB hydrogenation over Ir-Mo/Al<sub>2</sub>O<sub>3</sub> as a function of (a) [NB] and (b)  $P_{\text{H}_2}$ . Double logarithmic plot of the initial reaction rate of ST hydrogenation over Ir-Mo/Al<sub>2</sub>O<sub>3</sub> as a function of (c) [ST] and (d)  $P_{\text{H}_2}$ . Reaction conditions: NB or ST (0.025–0.1 mmol), H<sub>2</sub> (0.15–0.6 MPa), toluene (1 mL), Ir-Mo/Al<sub>2</sub>O<sub>3</sub> (10 mg, Ir: 0.52 mol%), and 303 K.

Table S4. Reaction orders of hydrogenation of NB and ST.

Catalyst	Nitrobenzene (NB)		Styrene (ST)	
	[NB]	$P_{H_2}$	[ST]	$P_{H_2}$
$Ir_4Mo_4/Al_2O_3$	$0.04 \pm 0.07$	$0.97 \pm 0.09$	$0.29 \pm 0.11$	$0.04 \pm 0.02$
$Ir-Mo/Al_2O_3$	$0.63 \pm 0.11$	$0.91 \pm 0.03$	$0.72 \pm 0.08$	$1.04 \pm 0.03$

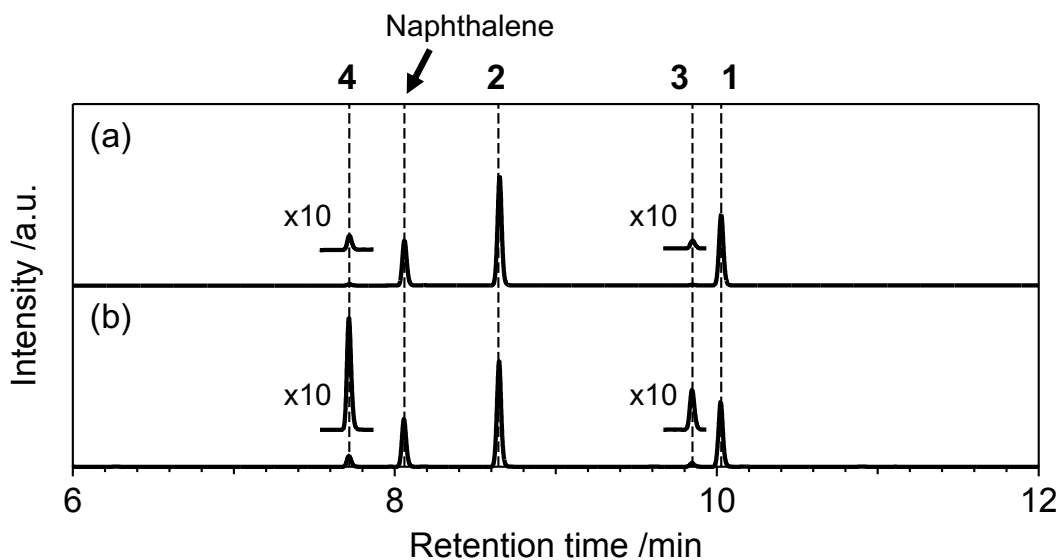


Figure S9. Representative GC chart of hydrogenation of **1** catalyzed by (a)  $Ir_4Mo_4/TiO_2$  (Conv. 61%, Select. 98%) and (b)  $Ir-Mo/TiO_2$  (Conv. 66%, Select. 87%). Reaction conditions: **1** (0.1 mmol),  $H_2$  (0.3 MPa), toluene (1 mL), catalyst (10 mg, Ir: 0.52 mol%), 303 K, and 10 min.